Two-dimensional phase-field simulation of self-assembled quantum dot formation

Takaki, Tomohiro
Hasebe, Tadashi
Tomita, Yoshihiro

Two-dimensional phase-field simulation of self-assembled quantum dot formation

Tomohiro Takaki [a, *], Tadashi Hasebe [b], Yoshihiro Tomita [b]
[a] *Faculty of Maritime Sciences, Kobe University, Kobe, 658-0022, Japan*
[b] *Faculty of Engineering, Kobe University, Kobe, 657-8501, Japan*

Abstract

The morphological evolution of a strained heteroepitaxial thin film of $Si_{1-x}Ge_x$/Si during deposition has been investigated by two-dimensional phase-field simulations. The phase-field model developed can form facet morphologies that are modeled using the generalized gradient correction coefficient for a crystal with a high anisotropy of surface energy, and can simulate the sequential shape transitions well known in the $Si_{1-x}Ge_x$/Si(001) system: a 2D wetting layer, faceted 3D pyramids, and multifaceted domes. The effects of Ge composition and mobility on island formation and island evolution have also been studied. Some typical and important phenomena observed in previous experimental studies during $Si_{1-x}Ge_x$/Si(001) heteroepitaxy have been simulated using the phase-field model.

Keywords : A1. Computer simulation, A1. Crystal morphology, A1. Growth models, A1. Nanostructures, B1. Germanium silicon alloys
PACS : 81.07.Ta, 81.15.Aa, 81.16.Dn

*Corresponding author
Tomohiro Takaki
Faculty of Maritime Sciences, Kobe University,
5-1-1, Fukaeminami, Higashinada, Kobe, 658-0022, Japan
Tel. : +81-78-431-4693, Fax : +81-78-431-6286
E-mail address : takaki@maritime.kobe-u.ac.jp

1. Introduction

The strain-induced self-assembly of islands in heteroepitaxial systems is a promising approach to the fabrication of quantum nanostructures for optoelectronic devices. The growth of SiGe alloy layers on Si(001) has been a subject of intense interest for the past years due to the fact that $Si_{1-x}Ge_x$/Si(001) serves as a model system for studying strain-driven transition.

In the $Si_{1-x}Ge_x$/Si(001) system, two-dimensional (2D) wetting layers transform into three-dimensional (3D) islands bounded by {105} faceted planes, i.e., pyramids [1]. With further Ge deposition, the pyramids undergo a morphological transition to dome-shaped islands with additional steeper {113} and {15 3 23} facets [2]. At a relatively high growth temperature, the same island transition is observed in a wide range of Ge fractions *x* [3] using different growth techniques. The Ge composition *x* mainly affects the size of the islands [4], which increases with decreasing *x*, and island formation. In fact, at a high *x*, islands are formed by nucleation [5], while at a low *x* ($x < 0.6$), individual islands are formed without nucleation from a quasiperiodic array of ripples as a result of strain-driven instability [6, 7]. Furthermore, a recent study has shown that, in dilute SiGe islands, a coherent barn island is formed following the formation of pyramid and dome islands, in which steep {111} facets are introduced [8].

As described above, island formation and island morphological evolution are largely affected by *x* and substrate temperature. To appropriately control the density, size distribution, spatial ordering, and shape of islands, it is necessary to conduct more systematic studies of the above-mentioned growth parameters. In this study, phase-field simulations are performed to investigate the effects of the growth parameters on island formation and island morphological evolution during deposition. In the phase-field model developed, facet morphologies are modeled using the generalized gradient correction coefficient for a crystal with a high anisotropy of surface energy [9]. Furthermore, to enable computation of the island morphological change from faceted pyramids to multifaceted domes with increasing Ge coverage, we apply the sixteen-fold of the surface energy. The validity of the model developed is confirmed by comparing the numerical results demonstrated here with the reported experimental observations.

2. Phase-field model

We consider a system composed of a substrate with a semi-infinite thickness, a thin film grown on the substrate heteroepitaxially and a vapor phase. The morphologies of the thin film are assumed to be determined by the competition of the surface energy and the elastic strain energy. The Ginzburg-Landau-type free-energy functional of the system is assumed to have the form

$$F = \int_V \left\{ f_d(\phi) + f_e(\phi, \varepsilon_{ij}) + \frac{a^2}{2}|\nabla\phi|^2 \right\} dV \tag{1}$$

where ϕ is the phase field taking a value of 1 in the solid (= substrate + film) and 0 in the vapor phase, ε_{ij} is the strain tensor, and a represents the gradient correction coefficient. $f_d(\phi)$ and $f_e(\phi, \varepsilon_{ij})$ are the double-well potential and the elastic strain energy, respectively, and are defined by the following equations.

$$f_d(\phi) = Wg(\phi) \tag{2}$$

$$f_e(\phi, \varepsilon_{ij}) = \frac{1}{2} D_{ijkl}(\phi)(\varepsilon_{ij} - \varepsilon_{ij}^0)(\varepsilon_{kl} - \varepsilon_{kl}^0) \tag{3}$$

Here, W is the barrier height of the double-well potential $g(\phi) = \phi^2(1-\phi)^2$. ε_{ij}^0 is the initial strain due to the lattice mismatch between the substrate and the thin film. $D_{ijkl}(\phi)$ denotes the elastic coefficient, which takes 0 in the vapor phase and D^0_{ijkl} in the solid phase and varies continuously in the surface region. $D_{ijkl}(\phi)$ is represented by

$$D_{ijkl}(\phi) = \rho(\phi) D^0_{ijkl} \tag{4}$$

where $\rho(\phi)$ indicates the density of the solid phase. We can change the distributions of the elastic coefficient by adjusting τ in the following equation [10].

$$\rho(\phi) = \frac{1}{2}\left[\tanh\frac{2\phi - 1}{2\tau} + 1 \right] \tag{5}$$

The surface anisotropy is taken into account using the following equation.

$$a(\theta)=\bar{a}\{1+\gamma\cos k\theta\} \tag{6}$$

Here, $\bar{a}$ is a constant related to the surface energy σ and the surface thickness δ, γ is the strength of anisotropy, k is the mode number, and θ is the angle between the surface normal and the x-axis. For values of high anisotropy such as $\gamma > 1/(k^2\text{-}1)$, the polar plot of $1/a$ is nonconvex when $a + a_{\theta\theta} < 0$, where the subscript θ denotes a derivative with respect to θ, and corresponding high-energy orientations are excluded from the equilibrium shape. The range of missing orientation is given by $(2\pi i/k\text{-}\theta_m) < \theta < (2\pi i/k+\theta_m)$, where i denotes integers from 0 to k-1 and the corner angle of the equilibrium shape or the first missing orientation θ_m is calculated from

$$a(\theta_m)\sin\theta_m + a_\theta(\theta_m)\cos\theta_m = 0 \tag{7}$$

In order to provide the equilibrium morphology without so-called "ears" corresponding to the missing orientation, we use the regularized gradient correction coefficient for the region of the missing orientation [9].

$$a(\theta)=\begin{cases}\bar{a}\{1+\gamma\cos k\theta\} & \text{for } (2\pi i/k+\theta_m)\le\theta\le(2\pi(i+1)/k-\theta_m)\\ \dfrac{a(\theta_m)}{\cos\theta_m}\cos\theta & \text{for } (2\pi i/k-\theta_m)<\theta<(2\pi i/k+\theta_m)\end{cases} \tag{8}$$

Here, we adopt the anisotropy mode k = 16, or sixteen-fold anisotropy, in order to simulate the multifaceted island and its morphological change. Figure 1 illustrates two-dimensional equilibrium shapes ($0\le\theta\le\pi/2$) drawn using the Gibbs-Thomson equation and Wulff's theorem [9] when k = 16 and γ = 0.02 which is larger than $1/(k^2\text{-}1)$. The drawings have so-called "ears" that do not belong to the equilibrium shape corresponding to the gray region. The introduction of the sixteen-fold surface energy anisotropy can define the angles between the x-axis and the faceted surface, θ_1 = 11.3˚, θ_2 = 33.8˚ and θ_3 = 56.3˚, which are close to the angles between the x-axis and {105}, {15 3 23} and {111} facets, i.e. 11.3˚, 33.6˚ and 54.7˚, respectively.

The following time-dependent Ginzburg-Landau equations considering the effects of anisotropy and deposition can be obtained.

$$\begin{aligned}\frac{\partial\phi}{\partial t} &= \nabla\left(M\nabla\frac{\delta F}{\delta\phi}\right)+V_d n_y\chi\\ &= M\nabla^2\left[2\phi(1-\phi)(1-2\phi)W+\frac{\partial f_e(\phi,\varepsilon_{ij})}{\partial\phi}+\frac{\partial}{\partial x}\left(a\frac{\partial a}{\partial\theta}\frac{\partial\phi}{\partial y}\right)-\frac{\partial}{\partial y}\left(a\frac{\partial a}{\partial\theta}\frac{\partial\phi}{\partial x}\right)-a^2\nabla^2\phi\right]+V_d n_y\chi\end{aligned} \tag{9}$$

Here, the phase field ϕ is assumed to be a conserved parameter. M is the mobility representing the surface diffusion. V_d, n_y and χ are the deposition rate, the y-direction component of the surface normal and a random number, respectively. We assume the stress equilibrium conditions $\sigma_{ij,j}$ = 0, since the elastic relaxation occurs much faster than the surface diffusion.

The constants $\bar{a}$ and W are related to the surface energy σ and the surface thickness δ by considering the one-dimensional steady-state condition: $\bar{a}=\sqrt{3\delta\sigma/b}$, $W = 6\sigma b/\delta$ [11]. Assuming the surface region is $\lambda < \phi < (1\text{-}\lambda)$, we obtain $b=2\tanh^{-1}(1-2\lambda)$ where, λ is the value of ϕ at the onset of surface region, such as λ = 0.1.

3. Numerical Simulation

The governing equations for phase field and stress field are discretized spatially using the finite difference method as a two-dimensional problem and the finite element method with isoparametric quadrilateral elements as a plane strain problem, respectively. We employ explicit time differencing on the phase-field equation.

Figure 2 shows the computational domain and boundary conditions. In Fig. 2, t_s represents the substrate thickness. The initial conditions for the phase-field variable are given by

$$\phi_{ini} = \frac{1}{2}\left[\tanh\left\{ \frac{b}{\delta}(t_s - y) + 1 \right\} \right] \tag{10}$$

The lattice mismatch strain ε^{mis} in the thin film is expressed as $\varepsilon^{mis} = (a_f - a_s)/ a_s$, where a_s and a_f are the lattice constants of the substrate and thin film, respectively. Here, it is convenient to apply the mismatch strain not to the thin film but to the substrate. The initial strain is, therefore, set to $\varepsilon_x^0 = - \{1 - \rho(\phi)+\rho_{\mathrm{ini}}(\phi)\}\ \varepsilon^{mis}$ in which $\rho_{\mathrm{ini}}(\phi)$ is the initial density of the solid phase, i.e., the density of substrate.

When Eq.(9) is solved explicitly, a very small time increment dt ($<< dx^4/a^2M$) and many time steps are required. In order to conduct the simulation efficiently, therefore, some numerical techniques given below are introduced in the present study. The phase-field equation, Eq.(9), is solved in the regions that include the vapor phase, the thin film and a part of the substrate, and for the calculation of the stress field, the coarse meshes ($9dx$ a side) are used in the substrate, which corresponds to the region where the phase field is not solved, as shown in Fig. 2. The lattice size for solving the phase field equation is the same as the size of the finite element for the stress field. The stress field is calculated every 100 steps of phase field calculation.

We assume periodic boundary conditions for phase field at both sides, and zero flux condition on the upper and lower ends, respectively. The displacements along the left-hand side and lower end of the computational domain are fixed in the x and y-directions, respectively. The displacement $-dX\ \varepsilon^{\mathrm{mis}}$ is applied to the right-hand side of the domain, as shown in Fig. 2.

The following parameters are used in the present simulations: the length of the computational domain dX = 2.025 μm, the width of the domain dY = 0.625 μm, the size of the difference lattice and finite element $dx = dy$ = 0.005 μm, the substrate thickness t_s = 0.50 μm, the surface energy σ = 1.23 J/m^2, the surface thickness $\delta = 4dx$, Young's modulus E = 104 GPa, Poisson's ratio ν = 0.27 [10], the lattice mismatch strain $\varepsilon^{mis} = 0.04x$ which obeys the Vegard's law, the random number χ = [0.9, 1.1], λ = 0.1, and τ = 0.12. The strength of anisotropy γ is set to 0.1, and then θ_m is calculated to 10.86 ° . The time increment dt is determined $dt = dx^4/(62.0a^2M)$ by taking the stability of numerical simulation into consideration. Here, we assume the isotropic elastic body and use the same physical properties for the thin film and substrate.

4. Numerical Results and Discussion

Figures 3 and 4 show the time slices of surface morphology and stress distribution in the x-direction, σ_{xx}, at a deposition rate V_{d} = 0.01 nm/s for Ge/Si and $Si_{0.5}Ge_{0.5}$/Si, respectively. (a), (b) and (c) in both Figs. 3 and 4 represent the results for $M = 1\times10^{-24}$, 5×10^{-25} and 1×10^{-25} m^5/Js, respectively. Since the mobility M is a function of surface diffusion coefficient [12], an increase in M corresponds to the higher growth temperature.

At the early growth stage of Ge/Si illustrated in Fig.3, it is observed that 3D pyramid islands are formed by nucleation and that the number of nucleation sites increases with decreasing M. Although not shown here, $Si_{0.25}Ge_{0.75}$/Si islands are also formed by nucleation. On the other hand, as for the lower-mismatch-strain $Si_{0.5}Ge_{0.5}$/Si system illustrated in Fig. 4, surface perturbations occur over the entire 2D wetting layer, and then a quasi-periodic rippled surface morphology is formed. Individual islands are observed to form by the coalescence of ripples with increasing SiGe alloy coverage. From the above results for the 3D pyramid formation, it is concluded that, at a low mismatch strain, 3D pyramid islands are formed from surface ripples as a result of strain-driven instability, while at high mismatch strain, islands are formed by nucleation. Experimental results in Ref. [6] have shown that over a wide composition range, i.e., $0.2 < x < 0.6$, 3D islands form without nucleation, while at $x > 0.6$, conventional 3D island nucleation is observed. Therefore, the numerical results for island formation are in good agreement with the experimental observations.

In Figs. 3 (b) and (c), after nucleation, coarsening, i.e., Ostwald ripening, takes place: Some islands continue to grow while others shrink and disappear. With further Ge deposition, pyramids transform into multifaceted dome islands. Although pyramids coexist with domes for some time, all the islands finally become dome-shaped. Such island coarsening and morphological change from pyramid to dome is also

observed in Figs. 4 (a) and (b) for $x = 0.5$. However, the coarsening is not due to Ostwald ripening but to the coalescence of two adjacent islands. Furthermore, note that $Si_{0.5}Ge_{0.5}$ islands tend to show improved spatial ordering and a narrow size distribution compared to Ge islands. In previous experimental studies [6], the same behaviors have been observed and the ordered array and narrow size distribution of lower Ge composition islands are largely affected by the formation of islands from a quasiperiodic array of ripples, resulting from strain-driven instability and the nucleation induces spatial disorder and size fluctuations. However, in Fig. 4 (c), a different morphological change from those observed under other conditions is observable, that is, a rippled surface morphology continues to grow without the formation of individual islands. In the growth of a dilute SiGe layer at low temperatures, such a continuous rippled surface morphology has been observed in some experiments [13]. Comparing the final island morphologies, a higher mobility tends to decrease island density for both Ge and $Si_{0.5}Ge_{0.5}$ films [14].

5. Conclusions

The heteroepitaxial growth of $Si_{1-x}Ge_x$/Si(001) alloys during deposition are simulated by the phase-field method as a two-dimensional problem, which is developed so as to simulate a typical sequential growth of a wetting layer, faceted pyramid islands and multifaceted dome islands. The effects of Ge composition and mobility on island formation and the evolution of surface morphology are investigated. It is confirmed that the phase-field model developed here can simulate some typical and important phenomena for the formation and evolution of SiGe islands grown on Si, as observed in previous experiments. We believe that this model can be applied to the analysis of other heteroepitaxial systems for the formation of faceted 3D islands and can be expanded to solve more realistic three-dimensional problems.

References

[1] Y.-W. Mo, D.E. Savage, B. S. Swartzentruber, M. G. Lagally, Phys. Rev. Lett. 65 (1990) 1020.
[2] F.M. Ross, R.M. Tromp, M. C. Reuter, Science 286 (1999) 1931.
[3] A. Rastelli, H. von Känel, Surf. Sci. 532-535 (2003) 769.
[4] W. Dorsch, H.P. Strunk, H. Wawra, G. Wagner, J. Groenen, R.Carles, Appl. Phys. Lett. 72 (1998) 179.
[5] J. Tersoff, F.K. LeGoues, Phys. Rev. Lett. 72 (1994) 3570.
[6] R.M. Tromp, F.M. Ross, M.C. Reuter, Phys. Rev. Lett. 84 (2000) 4641.
[7] P. Sutter, M.G. Lagally, Phys. Rev. Lett. 84 (2000) 4637.
[8] J.L. Gray, N. Singh, D.M. Elzey, R. Hull, Phys. Rev. Lett. 92 (2004) 135504-1.
[9] J.J. Eggleston, G.B. McFadden, P.W. Voorhees, Physica D 150 (2001) 91.
[10] Y.U. Wang, Y.M. Jin, A.G. Khachaturyan, Acta Mater. 52 (2004) 81.
[11] T. Takaki, T. Fukuoka, Y. Tomita, J. Crystal Growth (2005) *in print*.
[12] S.M. Wise, J.S. Lowengrub, J.S. Kim, W.C. Johnson, Superlattices and Microstructures 36 (2004) 293.
[13] J.A. Floro, E. Chason, L.B. Freund, R.D. Twesten, R.Q. Hwang, and G.A. Lucadamo, Phys. Rev. B 59 (1999) 1990.
[14] H.J. Kim, Z.M. Zhao, J. Liu, V. Ozolins, J.Y. Chang, Y.H. Xie, J. Appl. Phys 95 (2004) 6065.

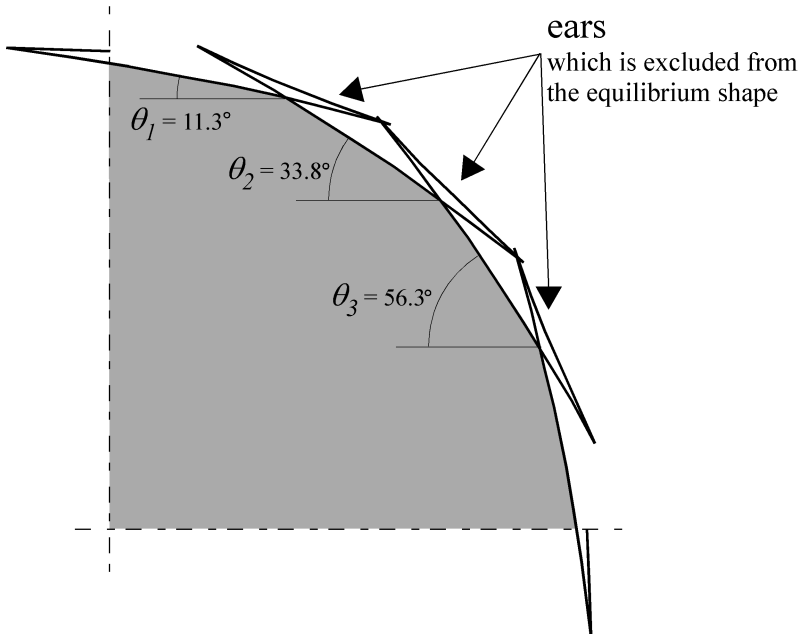

Fig. 1 Equilibrium shapes in the range of $0<\theta<\pi/2$ for k = 16 and γ = 0.02. The angles corresponding to "ears" are excluded from the equilibrium shape. Each planes can define the angles θ_1 = 11.3˚, θ_2 = 33.8˚ and θ_3 = 56.3˚.

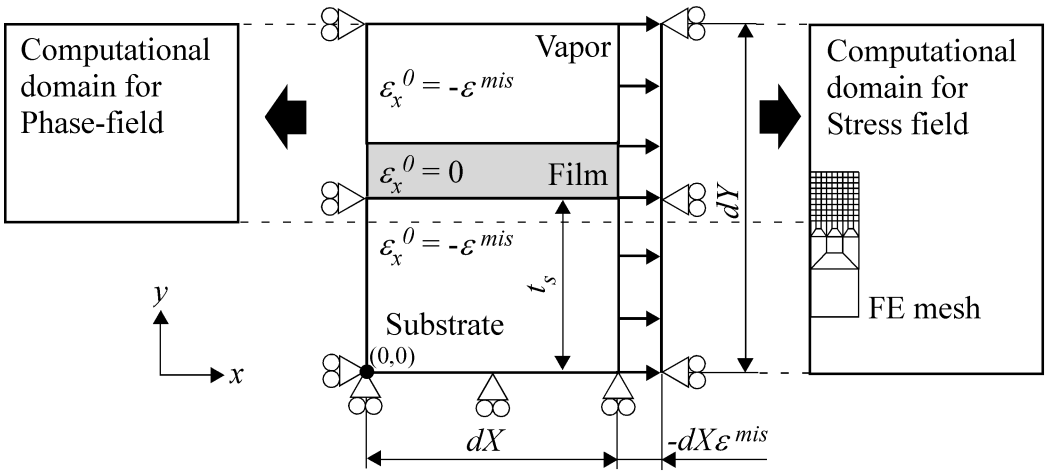

Fig. 2 Computational domains and boundary conditions. Center is the boundary conditions for the stress field. Phase field is solved in the vapor phase, the thin film and a part of the substrate. For the calculation of the stress field, the coarse meshes are used in the substrate.

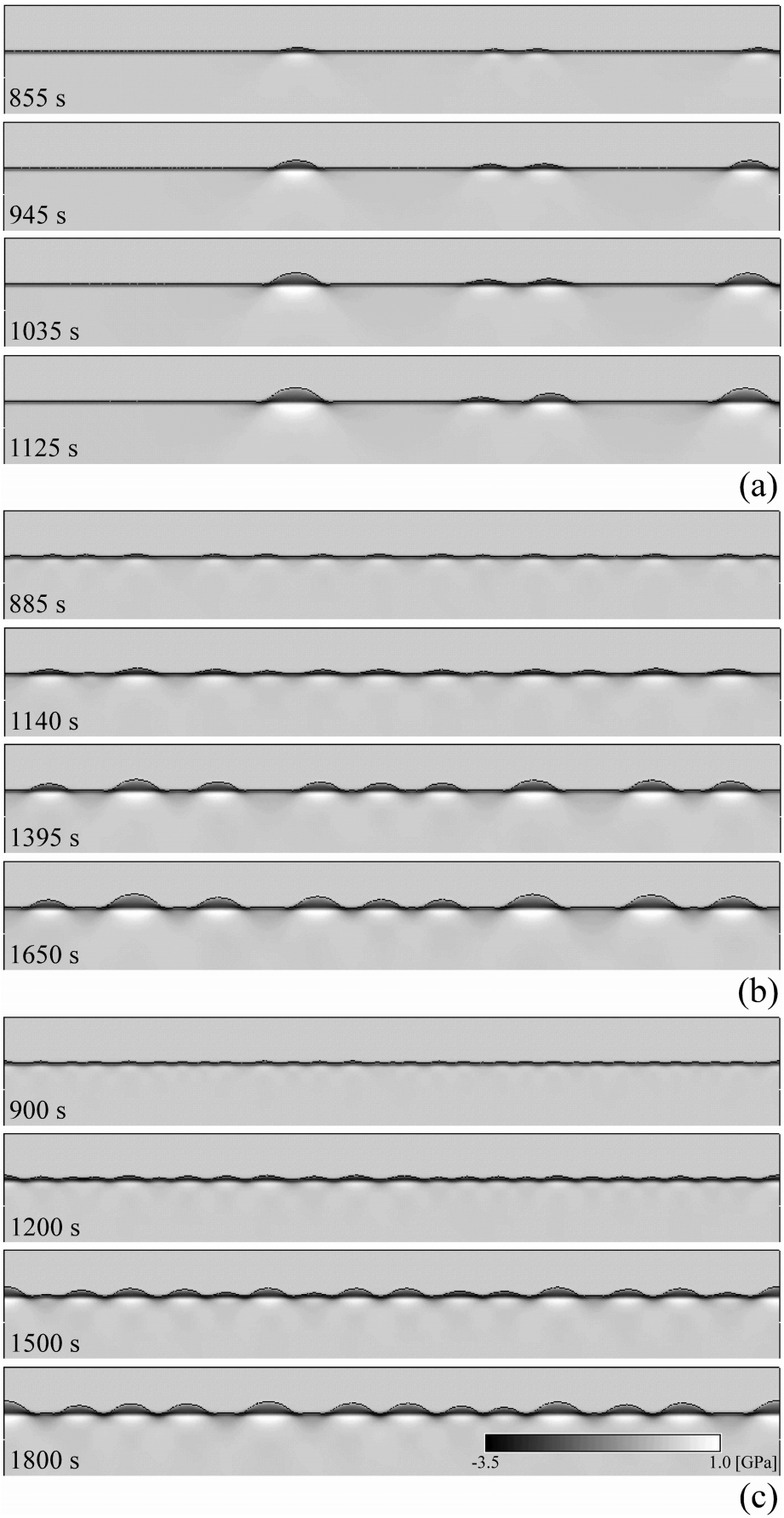

Fig. 3 Time slices of surface morphology and stress distribution σ_{xx} for Ge/Si system. (a) $M = 1\times10^{-24}$, (b) 5×10^{-25} and (c) 1×10^{-25} m^5/Js

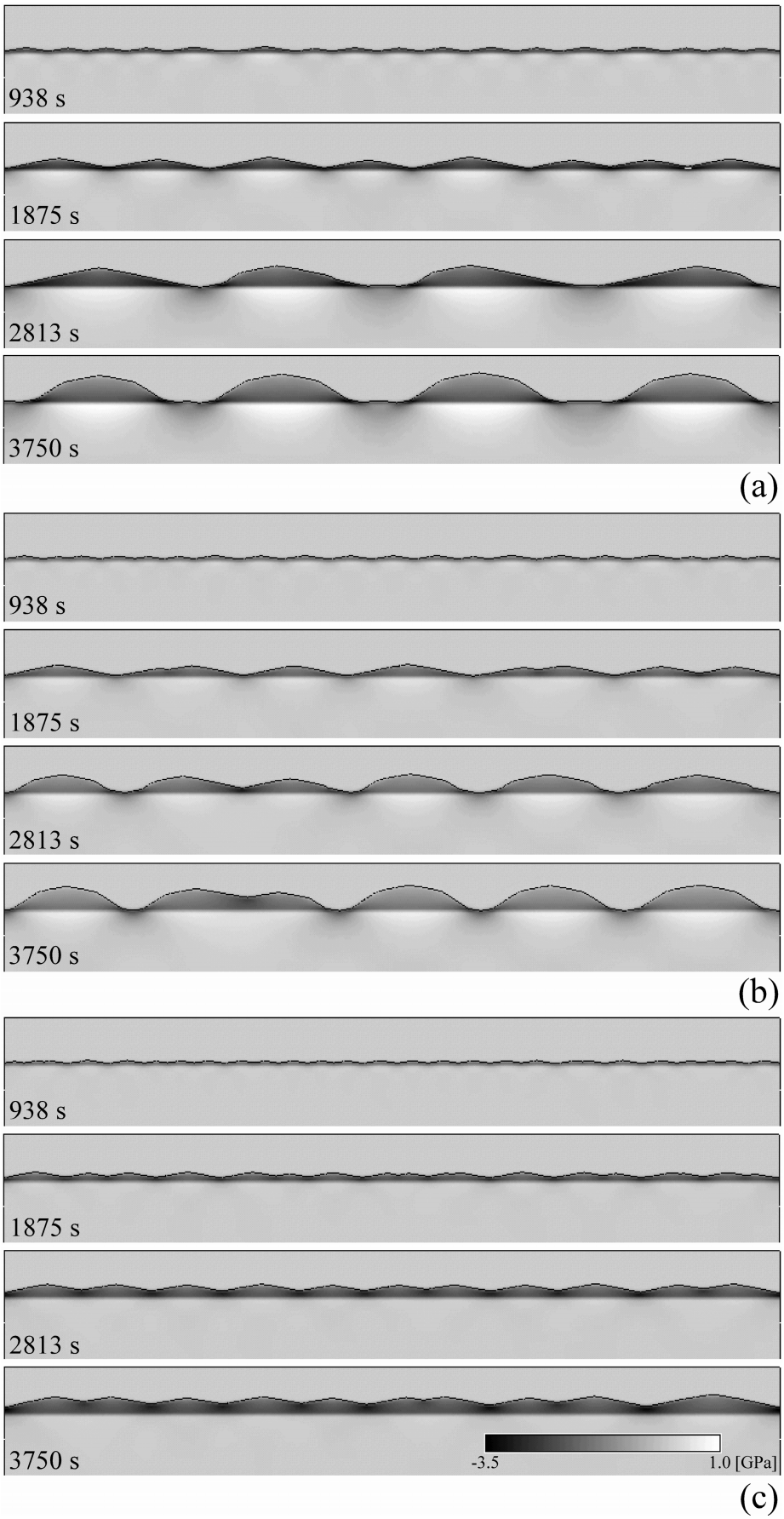

Fig. 4 Time slices of surface morphology and stress distribution σ_{xx} for $Si_{0.5}Ge_{0.5}$/Si system. (a) $M = 1\times10^{-24}$, (b) 5×10^{-25} and (c) 1×10^{-25} m^5/Js